ROYAL SOCIETY
OF CHEMISTRY

www.rsc.org/materialsC

Journal of Materials Chemistry C

RSCPublishing

ARTICLE

Red emissive diarylboron diketonate crystals: aggregation-induced color change and amplified spontaneous emission

Lu Wang, Zhenyu Zhang, Xiao Cheng, Kaiqi Ye, Feng Li, Yue Wang and Hongyu Zhang*

Two novel diarylboron diketonates **1** and **2** were synthesized by the reaction of 1,3-diaryl-β-diketone with triphenylborane or fluorobis(pentafluorophenyl)borane. The synthesized boron-containing compounds exhibit intense greenish blue or green emissions in solution whereas red fluorescence in crystals, showing an aggregation-induced colour change character. Notably, the flake-like crystals of **1** and **2** show obviously narrowed emission when irradiated by pulsed laser beam and thus provides the first example of amplified spontaneous emission based on four-coordinate organoboron solids. This finding indicates the potential of four-coordinate boron species in organic solid lasing and thus may expand the application area of boron-containing materials.

1. Introduction

Organoborane reagents have high reactivity towards bitentate organic ligands due to the vacant p-orbital of boron atom, which can not only allow the formation of rigid four-coordinate boron-bridged ring but also cause the intramolecular electron delocalization of the π-system.[1] The produced ring-fused structures can effectively constrain the molecular rotations hence may intensify the emission. In addition, the rigidified π-system may lower the lowest unoccupied molecular orbital (LUMO) level in turn endows the formed boron-containing materials with high electron affinity.[2] The chemical structures of four-coordinate boron materials can be conveniently modified for desired properties by changing either the type of the ligands or the nature of the substituents. Indeed, many highly efficient four-coordinate boron materials with emission colours ranging from deep blue to far red have been recently constructed and some of them even display bright fluorescence in the solid forms.[3] However, boron-containing materials with efficient red fluorescence (quantum yield over 0.30) in the solid state are still very rare.[3b,3e]

Luminescent π-conjugated organic materials have been intensively studied in the past decades due to their applications in optoelectronics including organic light-emitting diodes (OLEDs) and organic solid-state lasers (OSLs).[4] Among which, boron compounds with four-coordinate geometry are promising luminescent materials and have been found wide applications in the fields of OLEDs, organic field-effect transistors (OFETs), and sensors. Hydroxyquinolinate boron derivatives[5], pyridylphenolate boron derivatives[6], N-heterocycle-phenolate

boron derivatives[7] and N-heterocycle-N-heterocycle boron derivatives[8], β-diketonate boron derivatives[9] and other boron species[10] have been designed and applied in OLEDs. Full-colour electroluminescence has been achieved based on these organoboron emitters and some of them perform well in OLEDs as either emitting materials or electron-transporting materials. In addition, four-coordinate organoboron compounds have been recently employed as photo-responsive[11] or imaging materials[12] which further expand the application area of boron-containing materials. Nevertheless, luminescent organoboron solids have not yet been found application in OSLs.

In this contribution, two novel boron diketonates **1** and **2** were synthesized (Scheme 1). Both organoboron compounds exhibit quite different emission colours in the solution and crystalline states, displaying an aggregation-induced emission colour change feature. Their emission behaviors and other fundamental properties have been carefully investigated. Interestingly, both compounds produce highly efficient red emissive crystals with flake-like morphology and suitable size for generating amplified spontaneous emission (ASE). The potential of these crystals as a candidate for organic solid-state laser is thus evaluated.
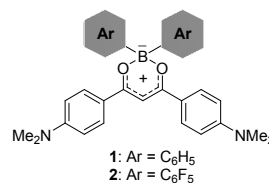
Scheme 1 Molecular structures of diarylboron diketonates **1** and **2**

2. Experimental section

2.1 materials and instruments

1,3-Diaryl-β-diketone and fluorobis(pentafluorophenyl)borane was synthesized according to the reported procedure.[13] Other starting materials were common commercial grade and used as received. The solvents for syntheses were freshly distilled over appropriate drying reagents. All experiments were performed under a nitrogen atmosphere using standard Schlenk techniques. IR spectra were recorded on a Bruker VERTEX 80v spectrometer. NMR spectra were recorded on a Bruker AVANCE 500 MHz spectrometer with tetramethylsilane as the internal standard. Mass spectra were recorded on a GC/MS mass spectrometer. Element analyses were performed on a FlashEA1112 spectrometer. UV−vis absorption spectra were recorded by a Shimadzu UV-2550 spectrophotometer. Melting points were determined on a Kofler hot−stage. The emission spectra of solutions were recorded by a ShimadzuRF-5301 PC spectrometer or a Maya2000 Pro CCD spectrometer. The absolute fluorescence quantum yields were measured on Edinburgh FLS920 using an integrating sphere. The fluorescence lifetimes were measured on Edinburgh FLS920 using a time-correlated single-photon (TCSPC) module. Cyclic voltammetries were performed on a BAS 100W instrument with a scan rate of 100 mV s^{-1}. A three-electrode configuration was used for the measurement: a platinum electrode as the working electrode, a platinum wire as the counter electrode, and an Ag/Ag$^+$ electrode as the reference electrode. A 0.1 M solution of tetrabutylammoniumhexafluorophosphate (TBAPF$_6$) in CH$_2$Cl$_2$ or DMF was used as the supporting electrolyte. Differential scanning calorimetric (DSC) measurements were performed on a NETZSCH DSC204 instrument at a heating rate of 10 °C min^{-1} under nitrogen. Thermogravimetric analyses (TGA) were performed on a TAQ500 thermogravimeter at a heating rate of 10 °C min^{-1} under nitrogen. Powder X-ray diffraction data were collected at 298K on a Bruker SMART-CCD diffractometer.

2.2 Synthesis of boron compounds 1 and 2

BPh$_3$ (3.5 mmol) or (C$_6$F$_5$)$_2$BF·OEt$_2$ (3.5 mmol) was added to a solution of (Z)-1,3-bis(4-(dimethylamino)phenyl)-3-hydroxyprop-2-en-1-one (3.2 mmol) in THF under nitrogen, the mixture was heated to reflux for 12 h. After cooling, the produced precipitates were filtered and recrystallized from CH$_2$Cl$_2$/MeOH 1:3 to yield the pure boron products.

Data of compound **1**. Yields: 82%. Mp: 314−315 °C. IR (υ$_{max}$/cm^{-1}) (KBr): 1606, 1546, 1493, 1431, 1377, 1349, 1253, 1191, 1169, 1133, 971, 877, 784, 704, 531. ^{1}H NMR (CD$_2$Cl$_2$, 500 MHz, ppm): δ 8.10 (d, J = 10.0 Hz, 4 H), 7.58 (d, J = 5.0 Hz, 4 H), 7.21 (t, J = 10.0 Hz, 4 H), 7.13 (t, J = 10.0 Hz, 2 H), 6.80 (t, J= 5.0 Hz, 5 H), 3.11 (s, 12 H). ^{13}C NMR (CD$_2$Cl$_2$, 125 MHz, ppm): δ 179.11, 154.55, 131.57, 130.64, 127.36, 126.20, 120.70, 111.59, 91.33, 40.32. MS m/z: 474.32 [M$^+$] (calcd: 474.25). Anal. Calcd (%) for C$_{31}$H$_{31}$BN$_2$O$_2$: C, 78.48; H, 6.59; N, 5.91; Found: C, 78.85; H, 6.43; N, 5.92.

Data of compound **2**. Yields: 69%. Mp: 325−326 °C. IR (υ$_{max}$/cm^{-1}) (KBr): 1607, 1552, 1501, 1437, 1373, 1287, 1254, 1191, 1172, 1091, 974, 791, 708, 559, 528. ^{1}H NMR (CD$_2$Cl$_2$, 500 MHz, ppm): δ 8.06 (d, J = 10.0 Hz, 4 H), 6.86 (s, 1H), 6.80 (d, J = 10.0 Hz, 4 H), 3.13(s, 12H). ^{13}C NMR (CD$_2$Cl$_2$, 125 MHz, ppm): δ 177.96, 155.01, 149.63, 141.28, 131.35, 119.50, 111.72, 90.67, 40.37. MS m/z: 654.18 [M$^+$] (calcd: 654.15). Anal. Calcd (%) for C$_{31}$H$_{21}$BF$_{10}$N$_2$O$_2$: C, 56.90; H, 3.23; N,4.28; Found: C, 57.39; H, 3.47; N, 4.31.

2.3 Computational details

Ab initio calculations were carried out with the Gaussian 09 program.[14] Geometry at ground state was optimized with the density functional theory (DFT) using the B3LYP functional and 6−31G(d,p) basis set.

2.4 Single crystal structure

Single crystal X-ray diffraction data were collected on a Rigaku RAXIS-PRID diffractometer using the ω-scan mode with graphite-monochromator Mo Kα radiation. The structures were solved with direct methods using the SHELXTL programs and refined with full-matrix leastsquares on F^2. Non-hydrogen atoms were refined anisotropically. The positions of hydrogen atoms were calculated and refined isotropically.

2.5 Amplified spontaneous emission measurement

For the laser test, the crystal slices were irradiated by the third harmonic (355 nm) of a Nd:YAG (yttrium–aluminum–garnet) laser at a repetition rate of 10 Hz and pulse duration of about 5 ns. The energy of the pumping laser was adjusted by using the calibrated neutral density filters. The beam was focused into a stripe whose shape was adjusted to 2 × 0.5 mm by using a cylindrical lens and a slit. The edge emission and PL spectra of the crystals were detected using a Maya2000 Pro CCD spectrometer. All the measurements were carried out at room temperature under ambient conditions.

3. Results and discussion

3.1 Synthesis and crystal growth

The boron diketonates were readily synthesized by refluxing the 1,3-diaryl-β-diketone with triphenylborane or fluorobis(pentafluorophenyl)borane in THF overnight. Cooling the reaction mixture to room temperature gives rise to the targets **1** and **2** as red crystals which can be isolated by a simple filtration in good yields (82% for **1** and 69% for **2**). The synthesized boron compounds have been fully characterized by NMR spectra, elemental analysis, IR and Mass spectra. For **1**, the crystalline sample generated by cooling the reaction mixture contains two polymorphs, red colour form **1a** with flake-like morphology and orange red colour form **1b** with block shape, which can be easily identified and separated due to their different colour and shape. Bulk red crystals (**2a**) with block shape based on compound **2** were obtained by vacuum sublimation. Solution diffusion method (CHCl$_3$/CH$_3$OH or

2 | *J. Mater. Chem*. C, 2014, **00**, 1-7

This journal is © The Royal Society of Chemistry 2014

CHCl$_3$/ether) only generates tiny flake-like crystals **2b** which are different to **2a** as confirmed by powder X-ray diffraction measurement (Fig. S1). Crystals **1a**, **1b** and **2a** have high quality and suitable size for X-ray diffraction analysis whereas **2b** cannot. The synthesized boron materials are thermally stable (Fig. S2 and S3) as reflected by their high melting points (314 ºC for **1** and 326 ºC for **2** measured by DSC) and decomposition temperatures (333 ºC for **1** and 337 ºC for **2** measured by TGA).

3.2 Optical properties

The optical properties of **1** and **2** in the solution and crystalline state have been fully investigated and compared. As shown in Fig. 1, the boron compounds show strong absorption bands peaking at 484 nm for **1** and 500 nm for **2**. The 16 nm difference between **1** and **2** reflects that different aryl groups at boron atom have a certain effect on the optical gap. To disclose the electronic structures of these diarylboron diketonates, density functional theory (DFT) calculations[14] using the B3LYP functional at the 6-31G(d,p) basis set have been performed. The highest occupied molecular orbitals (HOMO) and LUMO of **1** and **2** are both localized on the ligands (Fig. 2). Although the embedded boron moieties have little contribution to the molecular orbitals, they can affect the energy levels to a certain extent. The HOMO and LUMO levels of compound **2** are pulled down compared to those of **1**, clearly demonstrating the substituted effect. The HOMO-LUMO gap of 3.36 eV for **1** is slightly larger than that of 3.26 eV for **2**, consistent with the trend observed in absorption properties.

As shown in Fig. 1, compounds **1** and **2** exhibit highly efficient greenish blue and green fluorescence in CH$_2$Cl$_2$ (1.0 × 10^{-5} M) with emission bands peaked at 514 (2.85 ns) and 533 nm (3.59 ns), respectively. The emission spectrum of **2** is red shifted by about 20 nm compared to that of **1** due to the effect of electron-deficient pentafluorophenyl groups. The quantum yields of the solutions determined by an integrating sphere are in a high level, being 0.88 for **1** and 0.92 for **2**. Although the
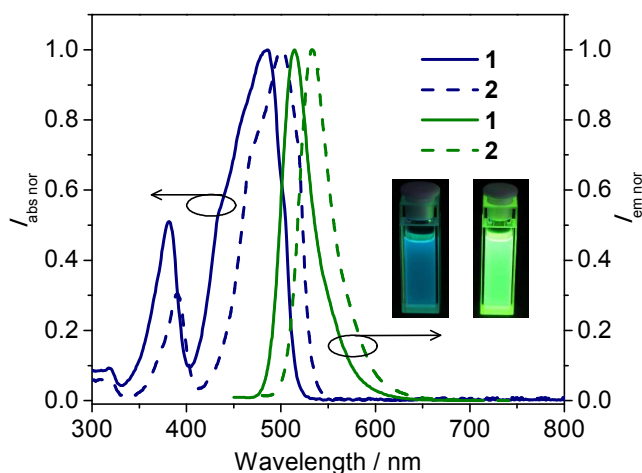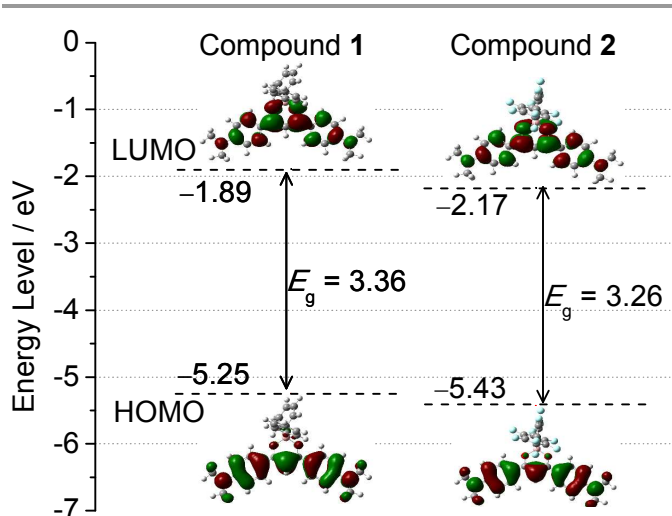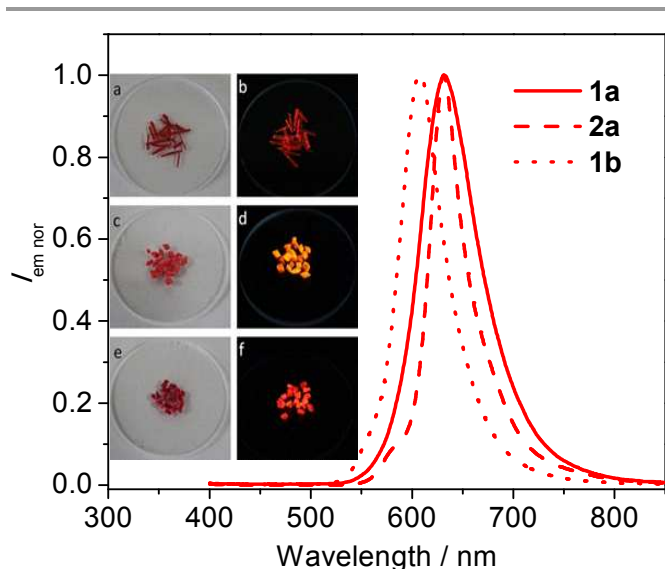

Fig. 2 Energy level alignment and pictorial drawings of HOMO and LUMO of boron compounds **1** and **2**.

skeleton of these boron compounds can be defined as a donor-acceptor structure, their emissions are assigned to $\pi^* \rightarrow \pi$ transition rather than intramolecular charge-transfer (ICT) on the basis of the weak solvent-dependent fluorescence spectra (Figs. S4 and S5).

The pale green solutions can form light red crystals by either solution diffusion or vacuum sublimation approaches. The crystalline samples of compound **1** by solvent diffusion approach contain two polymorphs **1a** and **1b** with different colours and morphologies (Inset in Fig. 3). The formed crystals **1a** and **2a** show strong red fluorescence with emission peaks at 630 (5.91 and 14.37 ns) and 631 nm (8.35 and 12.88 ns), respectively, which are dramatically red shifted by 116 and 98 nm compared to their CH$_2$Cl$_2$ solutions (Fig.3). Thus, these boron materials exhibit distinct green and red emission colours in solution and solid forms, respectively, displaying a aggregation-induced colour change feature. The quantum yields of the red emissive crystals **1a** and **2a** are 0.32 and 0.48, respectively. These values are indeed high for red emissive organic solids. Another polymorph **1b** show orange red fluorescence (607 nm) with quantum of 0.28. The emission band of **1b** is blue shifted by 23 nm compared to **1a**, presumably due to the different molecular conformation and/or packing manners which have been demonstrated to have great effect on solid-state fluorescence.[15] Notably, crystals **2a** shows very narrow photoluminescent (PL) spectrum with full widths at half-maximum (FWHM) of about 40 nm which is greatly smaller than that of **1a** (61 nm) and those of other red emitters. Although these boron materials are brightly red emissive in the crystalline phases, their thin films prepared by either spinning coating or thermally vacuum sublimation emit weak orange fluorescence (604 nm for compound **1** and 580 nm for compound **2**) with quantum yields of about 0.03 (Fig. S6). Thus, the present boron solids exhibit morphology-dependent emission property character.

Fig. 1 Absorption and emission spectra of compounds **1** and **2** (Inset: photographic images of solutions under 365 nm UV irradiation)

This journal is © The Royal Society of Chemistry 2014

J. Mater. Chem. C, 2014, **00**, 1-7 | **3**

Fig. 3 Optical properties of boron diketonates crystals (Inset: photographic images of crystals **1a** (a, b), **1b** (c, d) and **2a** (e, f) under daylight and 365 nm UV irradiation.).
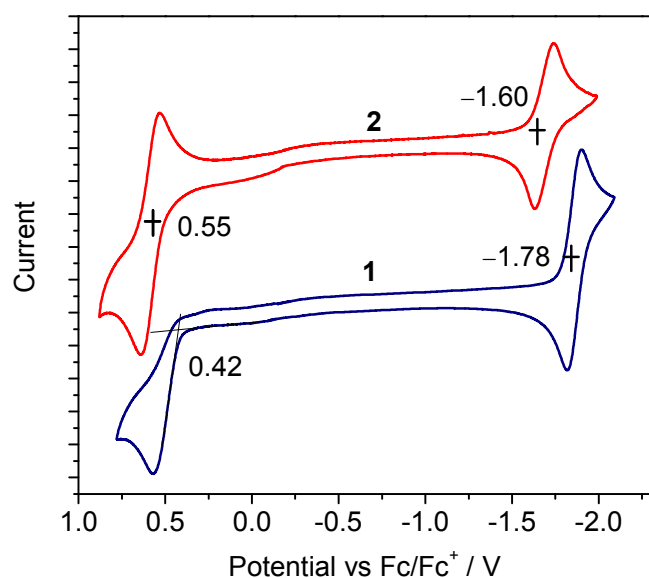
Fig. 4 Cyclic voltammograms of **1** and **2** measured with TBAPF$_6$ (0.1 M) as a supporting electrolyte at a scan rate of 100 mV s^{-1}.

3.3 Electrochemical properties

The redox processes of **1** and **2** were checked by means of cyclic voltammetry in DMF for reduction and CH$_2$Cl$_2$ for oxidation (Fig. 4). Both compounds display reversible reduction waves with half-wave potentials ($E_{red}^{1/2}$) of -1.78 V for **1** and -1.60 V for **2**, corresponding to the reduction of boron moieties. The reduction potential of **2** is positively shifted than that of **1**, reflecting that pentafluorobenzene increases the electron deficient nature of the boron material. The oxidation processes of dimethylamino group are irreversible for **1** and reversible for **2** with E_{ox}^{onset} of $+0.42$ V

and $E_{ox}^{1/2}$ of $+0.55$ V, respectively. Based on these data, the HOMO and LUMO are determined to be -5.22 eV and -3.02 eV for **1** and -5.35 eV and -3.20 eV for **2**.

3.4 Crystal structures

For a deep understanding of the interesting emission behaviors of these boron compounds, crystal structures of **1** and **2** were carefully investigated. Crystal **1a** and **2a** contains one individual molecule in the unit cell whereas crystal **1b** has three different constituent molecules. The molecular conformations of **1a** and **2a** are very similar, as shown in Fig. 5. Their bond lengths and angles of the boron bridged six-member rings and two B−C bonds are comparable, indicating that different aryl groups have insignificant effect on the coordinate ability of the boron atom. Due to the effective π−conjugation effect, the ligand moieties in both **1a** and **2a** take nearly the same planar skeleton. In addition, the four-coordinate geometry of the boron atoms as well as the location modes of the lateral phenyl rings in the individual molecules **1a** and **2a** is similar.
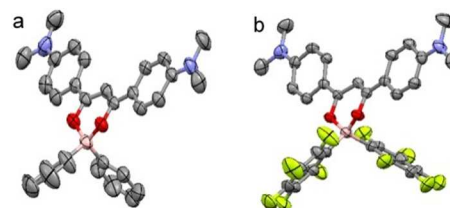
Fig. 5 Single-crystal X-ray diffraction structures of **1a** and **2a** (Thermal ellipsoids are shown at the 50% probability level and hydrogen atoms are omitted for clarity).

Although crystals **1a** and **2a** hold the very similar molecular conformations, their packing structures are totally different. In **1a**, two molecules oppositely approach together and form a dimer with intermolecular distance of 3.53 Å. The dimers pack into a chain structure along the crystallographic *b* direction through intermolecular π−π interactions (3.52 Å). The neighboring chains further generate a layer structure at *ac* plane in a herringbone fashion (Fig. 6a). In **2a**, the π−conjugated ligands of two molecules closely overlapped (3.70 Å), forming a molecular dimer which further interacted with neighboring dimers by π−π interactions (3.52 Å) and generate an infinite molecular chain along crystallographic *a* direction. The molecular chains are linked up in parallel by non-covalent C−H···F (2.60 Å) and C−H···π interactions (2.79 Å) and form a layer structure in *bc* plane (Fig. 6c). The general feature of crystal packing structures **1a** and **2a** is the formation of dimer and molecular chain structure which might be the major reason why the fluorescence of crystalline samples significantly red shift compared to that of the solutions. The small FWHM of crystal **2a** is presumably due to its high molecular rigidity as well as close molecular packing structure accompanied by multiple non-covalent intermolecular π−stacking, C−H···O and C−H···F hydrogen-bonding interactions (Fig. S7).

4 | *J. Mater. Chem.* C, 2014, **00**, 1-7

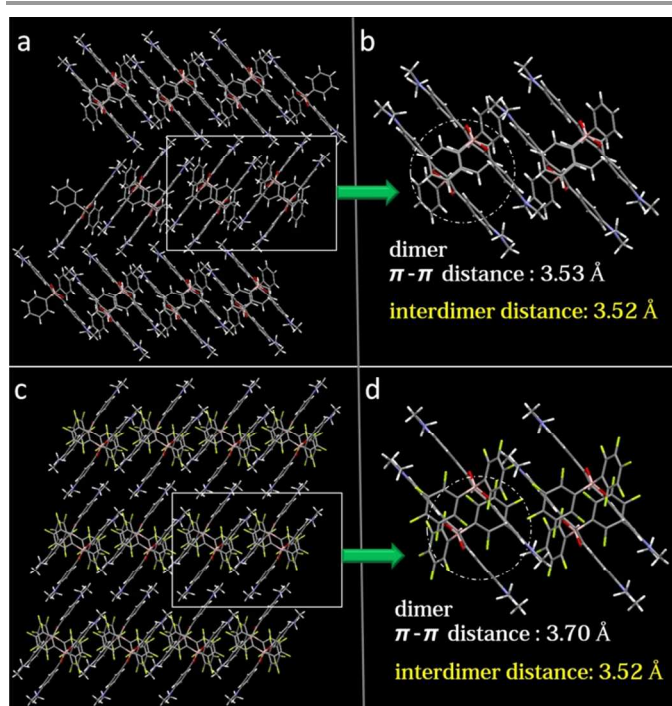This journal is © The Royal Society of Chemistry 2014

Fig. 6 Crystal packing structures and intermolecular interactions of **1a** (a and b) and **2a** (c and d).

Polymorphs **1a** and **1b** display red and orange red fluorescence, respectively. The constituent molecules of crystal **1b** also packed into layer structures in which the molecular chains are arranged in the parallel fashion. The emission colour difference between **1a** and **1b** is considered to be originated from their different molecular packing modes (Fig. S8).
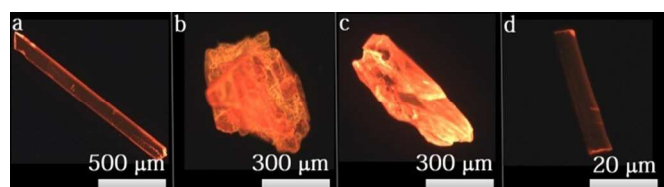
3.5 Amplified spontaneous emission

Fig. 7 Fluorescence microscope images of crystals **1a** (a), **1b** (b), **2a** (c), and **2b** (d).

High quality crystals accompanied with suitable morphology (co-planar facets) and high fluorescence efficiency are essential conditions for generating ASE or lasing.[16] Organic crystals that can produce red ASE are seldom reported so far due to the lack of efficient red emissive crystals with suitable size and shape. Fig. 7 shows the pictures of crystals **1a**, **1b**, **2a** and **2b** under UV irradiation (365 nm). As can be seen, the crystals **1a** and **2b** have regular edges as well as a relatively high-quality surface. And the edges of them give stronger emission as compared with the body surface, which indicates that the self-waveguided emission occurs. On the contrary, there are many cracks in crystals **1b** and **2a** and the emission is scattered out the crystals at the cracks. Thus, the self-waveguided effect cannot exist in crystals **1b** and **2a**. Generally, wave-guided

propagation of the emission is thought to be one prerequisite for ASE. Another factor that may affect the generation of ASE is molecular packing manner. The molecule chains are packed in a parallel mode in crystals **1b** and **2a** which is thought to be a negative factor for ASE due to the strong dipolar interactions.[17] In this sense, crystals **1a** and **2b** are possible candidates for generating ASE. Indeed, **1a** and **2b** are ASE-active whereas **1b** and **2a** cannot generate ASE upon irradiation by pulsed laser beam. To test the possibility of crystals **1a** and **2b** as red emissive lasing crystals, crystals **1a** and **2b** were irradiated by the third harmonic (355 nm) of a Nd:YAG (yttrium–aluminum–garnet) laser at a repetition rate of 10 Hz and pulse duration of about 5 ns and the emission spectra were collected in the edge area (Figs. 8 and 9). The nonlinear curves characterized by the peak intensity and pump energy (inset in Figs. 8 and 9) confirm the ASE behavior of polymorph **1a** and **2b**. Fig. 8 shows a comparison of the spectrum (**1a**) between PL and ASE irradiated by pulsed laser beam or UV light. The FWHM of the ASE spectrum is about 6.6 nm which is significantly narrowed compared to that of the normal PL spectrum (61 nm). The dependence of FWHM on the pump energy is shown in Fig. 8 (inset) which recorded the narrowing process of the emission spectra upon increasing the pump energy. Crystal **2b** displays similar emission behaviours when irradiated by pulsed laser beam. The dependence of FWHM on the pump energy and the comparison of spectrum between normal PL and ASE are shown in Fig. 9. The FWHM of emission significantly narrowed from about 36 nm to 9 nm when the pump energy increased. Interestingly, crystal **2b** shows much lower threshold value (842 kW/cm^2) than crystal **1a** (1950 kW/cm^2). This might be due to that in crystalline form compound **2** (quantum yields: 0.48 for **2a** and 0.50 for **2b**) is more intensely emissive than compound **1** (quantum yields: 0.32 for **1a** and 0.28 for **1b**).
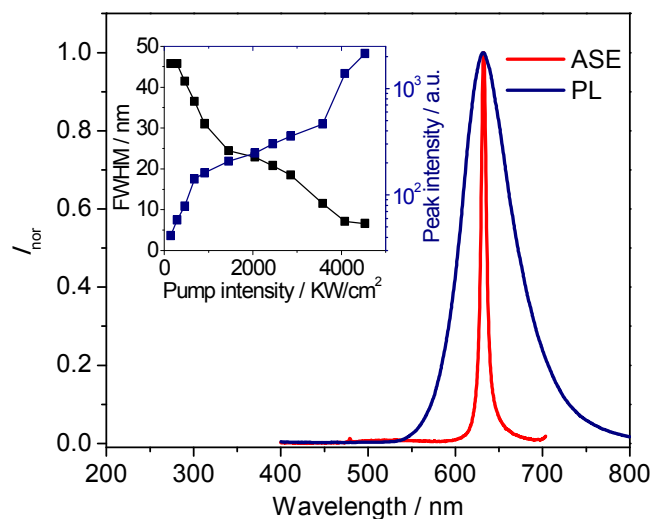

Fig. 8 Emission spectra of crystal **1a** under UV (PL) and laser irradiation (ASE). Insert: Dependence of the peak intensity and FWHM of emission spectra on the pump laser energy.
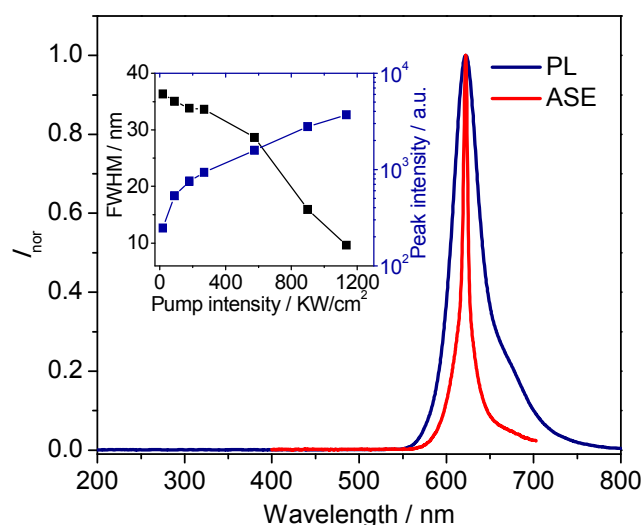
Fig. 9 Emission spectra of crystal **2b** under UV (PL) and laser irradiation (ASE). Insert: Dependence of the peak intensity and FWHM of emission spectra on the pump laser energy.

4. Conclusions

In summary, two novel diarylboron diketonates have been synthesized by a very simple approach. The produced boron materials exhibit highly efficient green fluorescence in solutions whereas red emissions in crystals, displaying an aggregation-induced colour change feature. Notably, the flake-like crystals of both boron compound exhibit self-waveguided emissions upon UV irradiation as well as amplified spontaneous emission irradiated by pulsed laser beam. This is the first example of boron-containing materials that show ASE character, to the best of our knowledge. Thus, the present study not only provides a rare example of organic crystals with highly efficient red fluorescence but also indicates the possible application of four-coordinate boron materials in organic solid-state lasers.

Acknowledgements

Notes and references

State Key Laboratory of Supramolecular Structure and Materials, College of Chemistry, Jilin University, Changchun 130012, P. R. China.
hongyuzhang@jlu.edu.cn

Electronic Supplementary Information (ESI) available: Optical, electrochemical and thermal properties, crystallographic data in PDF and CIF format as well as experimental details. See DOI: 10.1039/b000000x/
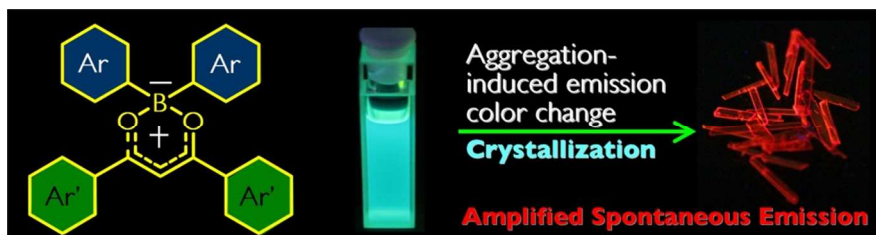
1   D. Li, H. Zhang, Y. Wang, *Chem. Soc. Rev.* 2013, **42**, 8416.
2   Y.-L. Rao, S. Wang, *Inorg. Chem.* 2011, **50**, 12263.
3   (a) D. Li, H, Zhang, C. Wagn, S. Huang, J. Guo, Y. Wang, *J. Mater. Chem.* 2012, **22**, 4319; (b) D. Li, K. Wang, S. Huang, S. Qu, X. Liu, Q. Zhu, H. Zhang, Y. Wang, *J. Mater. Chem.* 2011, **21**, 15298; (c) D. Li, Z. Zhang, S. Zhao, Y. Wang, H. Zhang, *Dalton Trans.,* 2011, **40**, 1279; (d) D. Li, Y. Yuan, H. Bi, D. Yao, X. Zhao, W. Tian, Y. Wang, H. Zhang, *Inorg. Chem.* 2011, **50**, 4825; (e) C.-L. Liu, Y. Chen, D. P. Shelar, C. Li, G. Cheng, W.-F. Fu, *J. Mater. Chem. C* 2014, **2**, 5471.
4   (a) Y. Hong, J. W. Y. Lam, B. Z. Tang, *Chem. Soc. Rev.* 2011, **40**, 5361; (b) A. Steffen, M. G. Tay, A. S. Batsanov, J. A. K. Howard, A. Beeby, K. Q. Vuong, X.-Z. Sun, M. W. George, T. B. Marder, *Angew. Chem. Int. Ed.* 2010, **122**, 2399; (c) J. C. Collings, A. C. Parsons, L. Porres, A. Beeby, A. S. Batsanov, J. A. K. Howard, D. P. Lydon, P. J. Low, I. J. S. Fairlamb, T. B. Marder, *Chem. Commun.* 2005, 2666; (d) J. R. Kumpfer, S. D. Taylor, W. B. Connick, S.t J. Rowan, *J. Mater. Chem.* 2012, **22**, 14196
5   (a) Y. Cui, Q.-D. Liu, D.-R. Bai, W.-L.; Jia, Y. Tao, S. Wang, *Inorg. Chem.* 2005, **44**, 601; (b) Y. Qin, I. Kiburu, S. Shah, F. Jäkle, *Org. Lett.* 2006, **8**, 5227; (c) Y. Cui, S. Wang, *J. Org. Chem.* 2006, **71**, 6485; (d) Y. Qin, C. Pagba, P. Piotrowiak, F. Jäkle, *J. Am. Chem. Soc.* 2004, **126**, 7015.
6   (a) H. Zhang, C. Huo, K. Ye, P. Zhang, W. Tian, Y. Wang, *Inorg. Chem.* 2006, **45**, 2788; (b) H. Zhang, C. Huo, J. Zhang, P. Zhang, W. Tian, Y. Wang, *Chem. Commun.* 2006, 281; (c) Z. Zhang, D. Yao, S. Zhao, H. Gao, Y. Fan, Z. Su, H. Zhang, Y. Wang, *Dalton Trans.* 2010, **39**, 5123.
7   (a) A. Wakamiya, T. Taniguchi, S. Yamaguchi, *Angew. Chem. Int. Ed.* 2006, **45**, 3170; (b) H.-J. Son, W.-S. Han, K.-R. Wee, J.-Y. Chun, K.-B. Choi, S. J. Han, S.-N. Kwon, J. Ko, C. Lee, S. O. Kang, *Eur. J. Inorg. Chem.* 2009, 1503.
8   (a) Q.-D. Liu, M. S. Mudadu, R. Thummel, Y. Tao, S. Wang, *Adv. Funct. Mater.* 2005, **15**, 143; (b) B. J. Liddle, R. M. Silva, T. J. Morin, F. P. Macedo, R. Shukla, S. V. Lindeman, J. R. Gardinier, *J. Org. Chem.* 2007, **72**, 5637; (c) D. Curiel, M. Más-Montoya, L. Usea, A. Espinosa, R. A. Orenes, P. Molina, *Org. Lett.* 2012, **14**, 3360.
9   (a) R. Yoshii, A. Hirose, K. Tanaka, Y. Chujo, *Chem. Eur. J.* 2014, **20**, 8320; (b) S. Xu, R. E. Evans, T. Liu, G. Zhang, J. N. Demas, C. O. Trindle, C. L. Fraser, *Inorg. Chem.* 2013, **52**, 3597; (c) P. Galer, R. C. Korošec, M. Vidmar, B. Šket, *J. Am. Chem. Soc.* 2014, **136**, 7383; (d) A. Nagai, K. Kokada, Y. Nagata, Y. Chujo, *Macromolecules* 2008, **41**, 8295; (e) A. Nagai, K. Kokado, Y. Nagata, M. Arita, Y. Chujo, *J. Org. Chem.* 2008, **73**, 8605; (f) G. Zhang, J. Lu, M. Sabat, C. L. Fraser, *J. Am. Chem. Soc.* 2010, **132**, 2160.
10   (a) A. Job, A. Wakamiya, G. Kehr, G. Erker, S. Yamaguchi, *Org. Lett.* 2010, **12**, 5470; (b) A. Fukazawa, H. Yamada, S. Yamaguchi, *Angew. Chem. Int. Ed.* 2008, **47**, 5582; (c) Y. Kubota, S. Tanaka, K. Funabiki, M. Matsui, *Org. Lett.* 2012, **14**, 4682; (d) Y. Kubota, H. Hara, S. Tanaka, K. Funabiki, M. Matsui, *Org. Lett.* 2011, **13**, 6544; (e) Y.-Y. Wu, Y. Chen, G.-Z. Gou, W.-H. Mu, X.-J. Lv, M.-L. Du, W.-F. Fu, *Org. Lett.* 2012, **14**, 5226; (f) X. Cheng, D. Li, Z. Zhang, H. Zhang, Y. Wang, *Org. Lett.* 2014, **16**, 880.
11   (a) Y.-L. Rao, C. Hőrl, H. Braunschweig, S. Wang, *Angew. Chem. Int. Ed.* 2014, **53**, 9086; (b) Y.-L. Rao, H. Amarne, S.-B. Zhao, T. M. McCormick, S. Matrić, Y. Sun, S.-Y. Wang, S. Wang, *J. Am. Chem. Soc.* 2008, **130**, 12898.
12   (a) G. M. Fischer, C. Jűngst, M. Isomäki-Krondahl, D. Gauss, H. M. Mőller, E. Daltrozzo, A. Zumbusch, *Chem. Commun.* 2010, **46**,

6 | *J. Mater. Chem.* C, 2014, **00**, 1-7

This journal is © The Royal Society of Chemistry 2014

5289; (b) G. Zhang, G. M. Palmer, M. W. Wewhirst, C. L. Fraser, *Nat. Mater.* 2009, **8**, 747.

13 (a) R. Duchateau, S. J. Lancaster, M. Thornton-Pett, M. Bochmann, *Organometallics* 1997, **16**, 4995; (b) N. M. Shavaleev, R. Scopelliti, F. Gumy, J-C. G. Bünzli, *Eur. J. Inorg. Chem.* 2008, 1523.

14 M. J. Frisch et al., Gaussian 09, Revision D.01, Frisch, Gaussian, Inc., Wallingford CT, 2009.

15 K. Wang, H. Zhang, S. Chen, G. Yang, J. Zhang, W. Tian, Z. Su. Y. Wang, *Adv. Mater.* 2014, **26**, 6168..

16 (a) H. Wang, F. Li, I. Ravia, B. Gao, Y. Li, V. Medvedev, H. Sun, N. Tessler, Y. Ma, *Adv. Funct. Mater.* 2011, **21**, 3770; (b) H. Mizuno, T. Maeda, H. Yanagi, H. Katsuki, M. Aresti, F. Quachi, M. Saba, A. Mura, G. Bongiovanni, F. Sasaki, S. Hotta, *Adv. Opt. Mater.* 2014, **2**, 529.

17 (a) M. Kasha, H. R. Rawls, M. A. EL-Bayoumi, *Pure. Appl. Chem.* 1965, **11**, 371; (b) F. Li, N. Gao, H. Xu, W. Liu, H. Shang, W. Yang, and M. Zhang, *Chem. Eur. J.* 2014, **20**, 9991.

Journal of Materials Chemistry C

ARTICLE

Graphical abstract

The present study not only provides a rare example of organic crystals with highly efficient red fluorescence but also indicates the possible application of four-coordinate boron materials in organic solid-state lasers.

Journal of Materials Chemistry C Accepted Manuscript